Radical Cation of Star-Shaped Condensed Oligofluorenes Having Isotruxene as a Core: Importance of Rigid Planar Structure on Charge Delocalization

ARTICLE *in* THE JOURNAL OF PHYSICAL CHEMISTRY A · MARCH 2014

Impact Factor: 2.69 · DOI: 10.1021/jp412744p · Source: PubMed

THE JOURNAL OF PHYSICAL CHEMISTRY A

Article

pubs.acs.org/JPCA

Radical Cation of Star-Shaped Condensed Oligofluorenes Having Isotruxene as a Core: Importance of Rigid Planar Structure on Charge Delocalization

Mamoru Fujitsuka,*[,†] Dae Won Cho,[†,‡] Sachiko Tojo,[†] Jungkweon Choi,[†] Hsin-Hau Huang,[§] Jye-Shane Yang,[§] and Tetsuro Majima*[,†]

[†]The Institute of Scientific and Industrial Research (SANKEN), Osaka University, Mihogaoka 8-1, Ibaraki, Osaka 567-0047, Japan

[‡]Department of Advanced Materials Chemistry, Korea University (Sejong Campus), Sejong 339-700, Korea

[§]Department of Chemistry, National Taiwan University, Taipei, Taiwan 10617

Supporting Information

ABSTRACT: Because of their excellent optical and electronic properties, oligofluorenes and polyfluorenes have been investigated for years. Recently developed star-shaped oligomers bearing a truxene or isotruxene core are interesting two-dimensional oligomers. Since employment of a condensed ring system will be effective in further extension of π-conjugation system, we studied electronic and vibrational properties of radical cation of CITF*n*, star-shaped condensed oligomer with isotruxene core and fluorene unit, by means of the radiation chemical methods. Absorption spectra of radical cation of CITF*n* were measured in the wide spectral range, which revealed extended π-conjugation of CITF*n*. Furthermore, time-resolved resonance Raman spectra during pulse radiolysis revealed that the oxidation of CITF*n* induced structural change to enhance quinoidal character. The Raman data and theoretical calculation indicated that the rigid framework of the present star-shaped oligomer which makes the oligomer a planar structure is quite important in extension of the conjugation pathway.

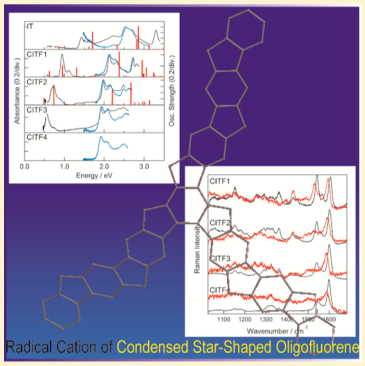

INTRODUCTION

Because of their excellent optical and electronic properties, oligofluorenes and polyfluorenes have been intensively investigated for years.[1−5] Recently developed star-shaped oligomers having a truxene (T) or isotruxene (IT) core are attractive two-dimensional oligomers, since T and IT core systems can be regarded as three overlapping fluorene units, which is effective to extend the conjugation pathway in a two-dimensional manner.[6−11] For these star-shaped oligomers, various optical and electronic properties characteristic to the extended π-electron system have been reported.[6−17] For understanding of their electronic properties, information on the charged state is indispensable. Therefore, we investigated absorption spectra of star-shaped oligofluorenes with a T or IT core (Supporting Information, Figure S1) in the previous study.[18] Absorption spectra of radical ion species in a wide spectral range were obtained and assigned to the electronic transitions adequately on the basis of time-dependent density functional theory (TDDFT). It was also predicted that these oligomers undergo structural change to take more planar structure upon oxidation or reduction.

To realize material with a further extended π-conjugation system, introduction of a completely planar π-electron system like graphenes will be a reasonable idea. In the case of star-shaped oligofluorene, application of a condensed ring system will realize a two-dimensional oligomer with an extended π-conjugated system. From this viewpoint, we have interests in the star-shaped condensed oligomer in Figure 1 (CITF*n*, *n* denotes number of benzene ring in a branch of oligomer except for the IT core), which is expected to take a completely planar structure preferable to the π-electron delocalization. In order to understand their charged state characteristic to the planar structure of CITF*n*, electronic and structural properties in the radical cation state have to be clarified.

For investigation of structural characteristics, vibration spectroscopies such as IR and Raman spectroscopies are quite powerful tools. Actually, for TF*n*, Oliva et al. reported detailed Raman spectroscopic study on both the neutral and oxidized states.[19] Because radical ions are usually transiently generated species, application of a spectroscopic method with better time resolution is preferable. From this reason, in the present study, we have combined time-resolved resonance Raman (TR^3) spectroscopy and the pulse radiolysis method, since TR^3 spectroscopy provides Raman spectra with high time resolution comparable to duration of the probe laser and pulse radiolysis can generate various radical ion species even when other methods, such as chemical and electrochemical reactions, cannot be applied.[20]

Here, we studied the radical cation of CITF*n* by theoretical and experimental methods based on the radiation chemistry.

Received: December 29, 2013
Revised: March 1, 2014
Published: March 5, 2014

   dx.doi.org/10.1021/jp412744p | *J. Phys. Chem. A* 2014, 118, 2307−2315

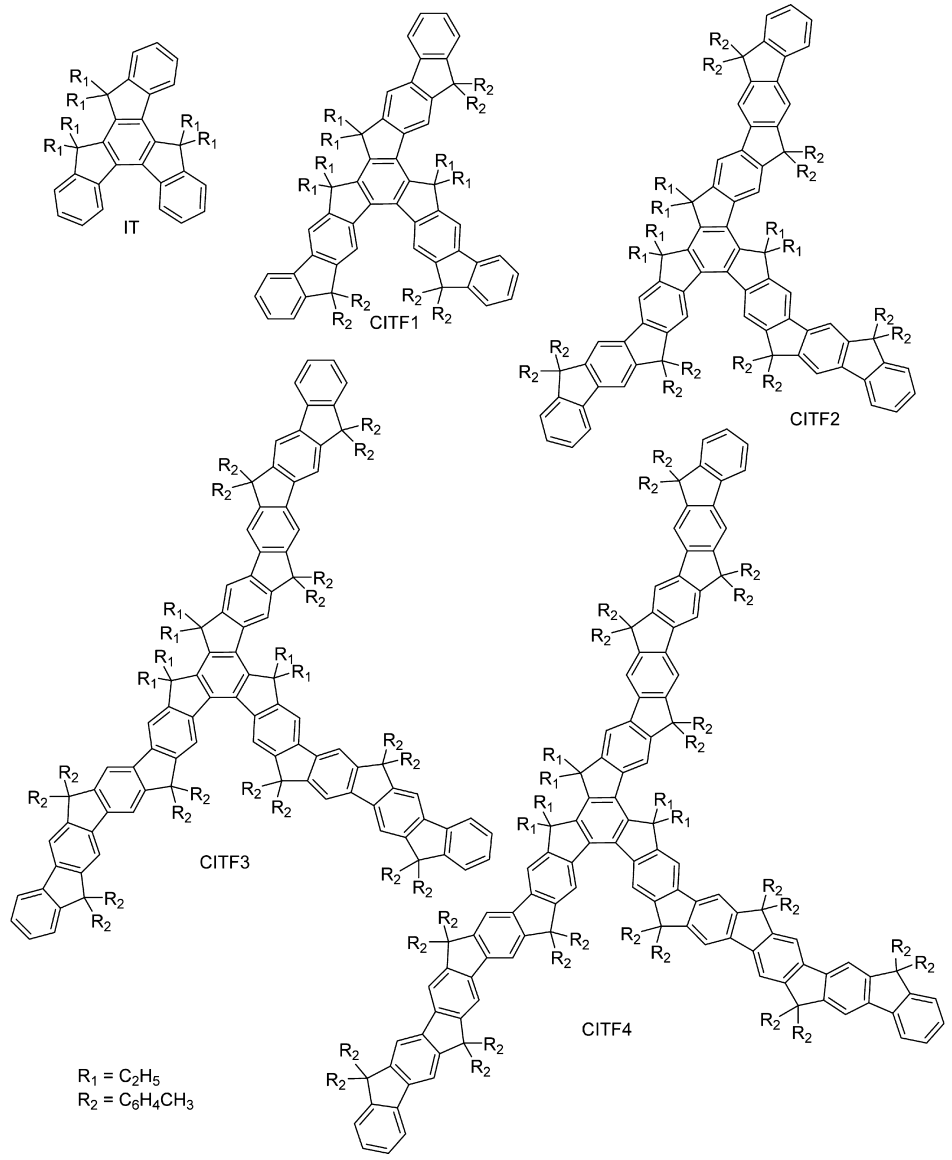

Figure 1. Molecular structures of CITF*n*.

Spectroscopic data were compared with those of ITF*n* and TF*n* as well as theoretical calculations. The obtained results revealed the importance of a rigid planar structure in extension of the π-conjugation pathway.

EXPERIMENTAL SECTION

Materials. TF*n*, ITF*n*, and CITF*n* were synthesized as indicated in the literature.[6−11] Solvents used in spectroscopic measurements were of the spectroscopic grades.

γ-Ray Irradiation to Frozen Matrix. The sample for γ-ray radiolysis (1 mM typically) was dissolved in *n*-butyl chloride (BuCl) to generate the corresponding radical cation. After the several freeze−pump−thaw cycles of the sample solution in a quartz cell (2 mm of optical path), the sample was kept at 77 K to form transparent glass and then subjected to γ-ray irradiation. The absorption spectra of the γ-ray irradiated sample at 77 K were measured using a Shimadzu UV-3100PC.

Transient Absorption Measurement during the Pulse Radiolysis. Pulse radiolysis experiments were performed using an electron pulse (28 MeV, 8 ns, 0.7 kGy per pulse) from a linear accelerator at Osaka University. In the present study, the sample (2 mM typically) was dissolved in 1,2-dichloroethane (DCE) in order to generate the radical cation of the sample. The transient absorption measurement during the pulse radiolysis was carried out using a nanosecond photoreaction analyzer system (Unisoku, TSP-1000). A pulsed 450 W Xe arc lamp (Ushio, UXL-451-0) was employed as a monitor light source. The monitor light passed through the sample solution was focused on the entrance slit of a monochromator (Unisoku, MD200) and detected with a photomultiplier tube (Hamamatsu Photonics, R2949) and a transient digitizer (Tektronix, TDS580D). The transient absorption spectra were measured using a photodiode array (Hamamatsu Photonics, S3904-1024F) with a gated image intensifier (Hamamatsu Photonics, C2925-01) as a detector.

Time-Resolved Resonance Raman (TR^3) Spectroscopy during the Pulse Radiolysis. The sample solution (2 mM typically) using DCE as a solvent was saturated with Ar gas and circulated through a quartz capillary tube with 2 mm internal diameter using a roller pump under Ar gas circumstance. An electron pulse from the above-mentioned accelerator (1 Hz repetition) was irradiated to the quartz capillary tube to which

dx.doi.org/10.1021/jp412744p | J. Phys. Chem. A 2014, 118, 2307−2315

the second harmonic generation (532 nm, 4 ns fwhm) of a ns Nd:YAG laser (Quantel, Brilliant) was irradiated as Raman excitation pulse in a collinear configuration after controlled delay time using a digital delay generator (Stanford Research Systems, DG535). Scattered light from the sample to the perpendicular direction with respect to the laser pulse was collected using appropriate lenses and focused onto the optical fiber, which guided the scattered light onto a slit of a polychromator (Princeton Instruments, Acton SP-2500i) equipped with a grating (1200 g/mm) after passing through an edge filter to remove Rayleigh scattering. The scattered light was detected with an ICCD detector (Princeton Instruments, PI-MAX3) operated with 5 ns of gate width, typically. All instruments were controlled using a personal computer via a controller (Unisoku). The Raman spectrum was obtained by accumulation of 1000 events typically. From the spectra, Raman peaks due to the solvent were removed by subtraction. In order to obtain Raman spectra of radical ions, Raman peaks from neutral substrate were subtracted from the spectra.

Steady State Absorption and Fluorescence Spectroscopy. Steady state absorption and fluorescence spectra of the sample were measured using Shimadzu UV-3100PC and Horiba FluoroMax-4P, respectively.

Theoretical Calculation. Optimized structures in the ground and radical cation states and Raman spectra of molecules in the present study were estimated by using density functional theory (DFT) at the B3LYP/6-31G(d) level. The excitation energies of the radical ions were estimated using time-dependent DFT (TDDFT) at the B3LYP/6-31G(d) level. All theoretical calculations were carried out using the Gaussian 09 package.[21] In the calculation, alkyl substituents were replaced by methyl group for simplicity of calculation. For ITF*n*, both anti and syn forms are expected with respect to the direction of fluorene units. For simplicity, all anti and all syn forms were calculated. It was confirmed that the estimated structures did not exhibit imaginary frequency.

RESULTS AND DISCUSSION

Steady State Absorption and Fluorescence Spectra of CITF*n*. Figure 2 shows steady state absorption spectra of CITF*n* in THF. Absorption peak positions (λ_{abs}) are summarized in Table 1. Each absorption spectrum comprised well-resolved vibrational bands. In addition, the absorption maximum appeared at the longest wavelength shifted to red as the size of the oligomer increased. These spectral features are obvious when compared with those of ITF*n*: ITF*n* showed rather broad absorption bands with obscure vibrational structure and their peak shift with the oligomer size was not obvious.[14] These results indicate a significant effect of the methylene linkages, which connect benzene rings and make the molecule configuration planar, resulting in extension of π-conjugation across the star-shaped oligomer.[10,11] In the case of neutral ITF*n*, it is indicated by the theoretical calculation that dihedral angles formed by the IT core and fluorene or fluorene–fluorene are about 36° due to the steric hindrance by Hs of benzene rings, which limits extension of the π-conjugation system.[18]

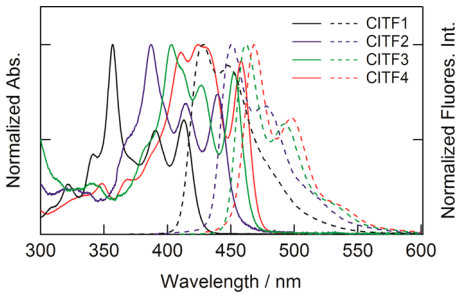

Figure 2. Absorption (solid lines) and fluorescence (broken lines) spectra of CITF*n* in THF.

Table 1. Observed Absorption and Fluorescence Peaks and Stokes Shift of Neutral CITF*n* (n = 1–4) in THF

	λ_{abs}/nm	λ_{fl}/nm	Stokes shift/cm^{-1}
CITF1	321, 342, 357, 390, 413	428, 447	849
CITF2	387, 418, 440	450, 478	606
CITF3	403, 427, 453	462, 493	430
CITF4	411, 424, 458	468, 498	466

Steady state fluorescence spectra of CITF*n* are also indicated in Figure 2 and Table 1. Well-resolved vibrational structures and peak shift with the oligomer size were also confirmed in the fluorescence spectra. It is also noted that the fluorescence peak positions (λ_{fl}) were located at longer wavelength when compared to the corresponding ITF*n*.[14] In Table 1, Stokes shifts estimated from the absorption and fluorescence spectra are also listed. It is obvious that the Stokes shift of CITF*n* is quite small when compared to those of ITF*n*. Furthermore, it is interesting to note that the Stokes shift of CITF*n* tends to become smaller with the size of oligomer. This fact indicates smaller structural change between the S_0 and the relaxed S_1 states of the larger CITF*n*.

Absorption Spectra of Radical Cations. In order to obtain absorption spectra of radical cations in a wide spectral range, absorption spectrum measurement of γ-ray irradiated CITF*n* in BuCl glassy matrix, which is a well-established method to generate radical cation of substrates and provides absorption spectra in a wide range from UV to near-IR,[20] was carried out. In Figure 3, absorption spectra of radical cations were indicated. For CITF1, CITF2, and CITF3, absorption spectra of radical cations were successfully obtained, while poor

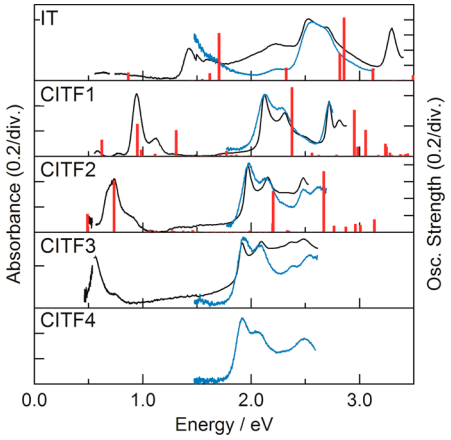

Figure 3. Absorption spectra of CITF*n* radical cations generated by γ-ray irradiation to the BuCl rigid matrix at 77 K. Transient absorption spectra at 100 ns after electron pulse during the pulse radiolysis of CITF*n* in DCE at room temperature are indicated by blue. Oscillator strengths calculated by TDDFT at the B3LYP/6-31G(d) level are indicated by red bars (see also Table 2).

dx.doi.org/10.1021/jp412744p | J. Phys. Chem. A 2014, 118, 2307–2315

Table 2. Observed Absorption Peaks, Calculated Transition Energies, Oscillator Strength (f), and Relative Contribution of Excited State Configuration of IT and CITFn (n = 1−4) Radical Cations[a]

	λ_{abs}/nm[b]	calcd E/eV	f	rel contribn of excited state confign[c]
IT	∼1960 (∼0.63)	0.866	0.027	0.97(HOMO−1(β) → HOMO(β))
	866 (1.43)	1.703	0.156	0.50(HOMO−5(β) → HOMO(β)) + 0.67(HOMO−4(β) → HOMO(β)) + 0.44(HOMO−3(β) → HOMO(β))
	490 (2.53)	2.857	0.207	0.73(HOMO(α) → LUMO(α)) − 0.53(HOMO−7(β) → HOMO(β))
CITF1	∼2130 (∼0.58)	0.623	0.109	0.98(HOMO−1(β) → HOMO(β))
	1314 (0.94)	0.950	0.214	0.95(HOMO−2(β) → HOMO(β))
	584 (2.12)	2.377	0.456	0.89(HOMO(α) → LUMO(α))
	456 (2.72)	2.952	0.307	0.69(HOMO−1(α) → LUMO(α)) − 0.32(HOMO−24(β) → HOMO(β)) + 0.54 (HOMO−1(β) → LUMO (β))
CITF2	>2490 (<0.50)	0.491	0.216	0.98(HOMO−1(β) → HOMO(β))
	∼1686 (∼0.74)	0.734	0.616	0.98(HOMO−2(β) → HOMO(β))
	630 (1.97)	2.202	0.488	0.77(HOMO(α) → LUMO(α)) + 0.30(HOMO−38(β) → HOMO(β))
	500 (2.48)	2.669	0.722	0.72(HOMO−1(α) → LUMO (α)) + 0.66 (HOMO−1(β) → LUMO(β))
CITF3	∼2220 (∼0.56)			
	646 (1.92)			
	500 (2.48)			
CITF4	648 (1.92)			
	498 (2.49)			

[a]Calculated at B3LYP/6-31G(d) level. Alkyl groups were reduced to methyl group. [b]Number in parentheses is peak position in eV unit. [c]Relative contribution larger than 0.3 is indicated.

solubility of CITF4 in BuCl at 77 K made absorption measurement impossible. The absorption peak positions of radical cations obtained by γ-ray radiation are summarized in Table 2.

In addition to γ-ray irradiation, we carried out the transient absorption measurements during the pulse radiolysis of CITFn in DCE (Figure S2 in the Supporting Information). Although the spectral range of the transient absorption is limited when compared to absorption measurement of the γ-ray irradiated sample, better solubility in room temperature solvent made absorption measurement possible. In Figure 3, transient absorption spectra measured during the pulse radiolysis were indicated by blue. For CITF4, the absorption spectrum of radical cation was successfully obtained. It is also indicated from Figure 3 that there is not a significant difference between spectra obtained by these two methods, although room temperature measurement caused slight peak broadening. In Table 2, for CITF4, peak positions obtained by the pulse radiolysis were indicated. It is also revealed from the transient absorption measurement during the pulse radiolysis that the generated radical cations of CITFn were quite stable and did not decay within a millisecond time window (Figure S2 in the Supporting Information, lower panel), probably because the backbone of CITFn makes stable radical cation formation possible and the $C_6H_4CH_3$ substituent groups at the methylene linker, which can cover the CITF backbone, inhibited the recombination process.[22]

For better understanding of these absorption bands, transition energies and oscillator strengths of CITFn radical cations were calculated using TDDFT at the B3LYP/6-31G(d) level. TDDFT calculations were limited to IT, CITF1, and CITF2 because of limitation of the present facilities. The calculated transition energies and oscillator strengths were summarized in Table 2 and indicated in Figure 3 as bars, which showed that the calculated transition energies explain the observed peak adequately. In the case of IT radical cation, absorption peaks appeared at ∼1960, 866, and 490 nm. The absorption peak at ∼1960 nm is attributed to the transition between HOMO−1 and HOMO (=SOMO), while the absorption at 490 nm is due to the transition between HOMO and LUMO mainly (Table 2). The absorption band at 866 nm includes contributions of the transitions from HOMO−n (n > 1) to HOMO. With the size of the oligomer, both near-IR and visible bands shifted to the lower energy (i.e., longer wavelength side). For CITF1 and CITF2, theoretical calculations indicated that the near-IR bands are due to the transition from HOMO−n ($n \geq 1$) to HOMO, while the visible band can be attributed to the transition between HOMO and LUMO. Although theoretical calculation on further larger oligomer was not carried out, their absorption spectra are similar to those of CITF1 and CITF2, indicating that the origins of absorption bands of the larger oligomers are the same as those of smaller oligomers.

It should be noted that these assignments of the absorption bands of radical cations are similar to those of ITFn radical cations.[18] From the comparison of peak position of radical cations, it is obvious that the peak position of the visible band of CITFn is located at longer wavelength side than those of ITFn (CITF2 (630 nm) vs ITF1 (550 nm) and CITF4 (648 nm) vs ITF2 (604 nm)). Because the visible absorption band of the radical cation is originated from the HOMO to LUMO transition, the result indicates well charge delocalization over CITFn when compared to ITFn.

Raman Spectra of ITFn. In Figure 4, Raman spectra of neutral ITFn are indicated by black. To assign these bands, theoretical calculation at B3LYP/6-31G(d) level was carried out. For ITFn, both syn and anti forms are expected with respect to the bond connecting core and fluorene or fluorene and fluorene units. For simplicity of the calculation, all syn and all anti forms were calculated. It was revealed that the all anti form is energetically slightly more stable than the all syn form (for example, the all anti form is stable more than the all syn form by 3.8 meV in the case of ITF1). It was also indicated that the calculated Raman bands were almost the same. Thus, the calculated vibrations of the anti form are referred in the following discussion. The most intense Raman signals of

dx.doi.org/10.1021/jp412744p | J. Phys. Chem. A 2014, 118, 2307−2315

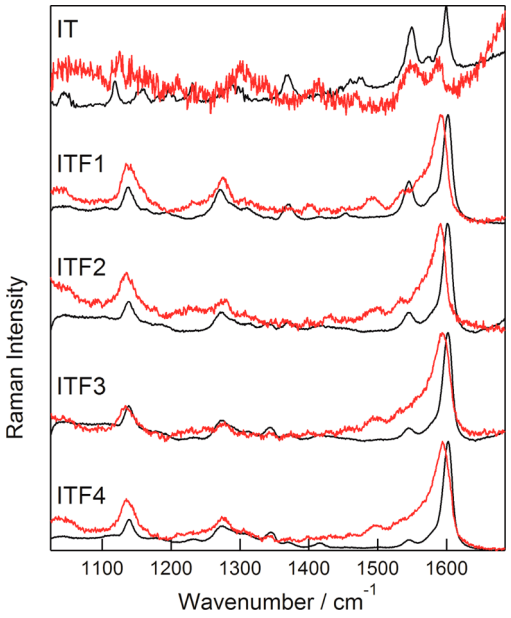

Figure 4. Raman spectra of neutral (black) and radical cation ITF*n* (red) in DCE. TR[3] spectra of radical cations were measured at 50 ns after electron pulse during the pulse radiolysis of ITF*n* in DCE.

neutral IT appearing in the 1500−1600 cm^{-1} region are attributed to C−C stretching modes of benzene rings. The 1600 cm^{-1} band arises from three C−C stretching modes of the external benzene rings (calcd: 1607, 1608, and 1609 cm^{-1}) and is almost the same position with that of T in DCE (Figure S3 in the Supporting Information, 1596 cm^{-1}). The shoulder at 1590 cm^{-1} resembles that of T,[19] indicating efficient conjugation nature of IT. Two Raman peaks at 1574 and 1549 cm^{-1} can be attributed to the C−C stretching modes of the inner benzene ring: Theoretical calculation predicted that these two peaks are at 1565 and 1546 cm^{-1}, respectively (Figure 5). It should be noted that T showed only a single Raman peak at 1544 cm^{-1} for these modes because two corresponding vibrations were calculated to have almost the same wavenumbers (1557 and 1558 cm^{-1}) in the case of T due to its symmetry. In addition to these bands, medium intensity bands were observed at 1369, 1287, 1231, 1196, 1156, and 1118 cm^{-1}. These bands resemble

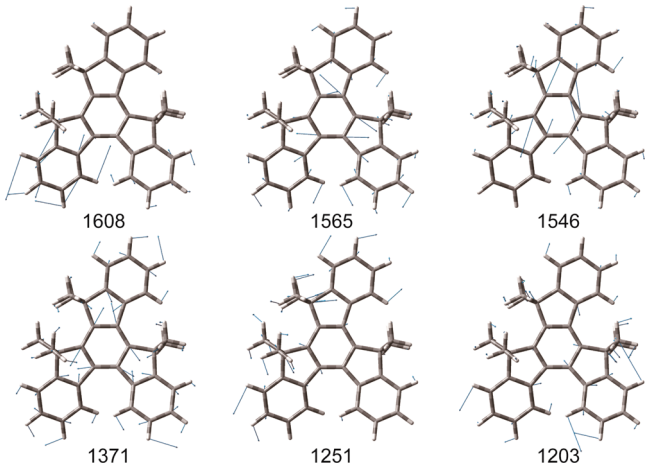

Figure 5. Representative atomic displacements of IT calculated at the B3LYP/6-31G(d) level. Numbers under molecules are calculated wavenumbers scaled using a factor (0.97).

those of T, which showed corresponding peaks at 1370, 1290, 1230, 1193, 1157, and 1121 cm^{-1} (Figure S3 in the Supporting Information), respectively. The theoretical calculation supported the similar spectral pattern in this region. These bands can be assigned as indicated in Table 3 based on the theoretical calculation (Figure 5) as well as the previous report on T.[19]

Table 3. Observed Raman Bands of Neutral ITF*n* in DCE

IT	ITF1	ITF2	ITF3	ITF4	assignment
1600	1602	1601	1602	1603	C−C stretch
1574					C−C stretch
1549	1546	1546	1544	1545	C−C stretch
1475					alkyl CH deformation
1460	1452				in-plane CH bend
		1419	1419	1416	in-plane CH bend
1369	1372	1371	1372	1369	symmetric C−C stretch
	1342	1344	1344	1345	C−C stretch (intrafluorene)
	1310	1312	1313	1308	C−C stretch (interfluorene)
1287					C−C stretch + CCC bend
	1271	1274	1276	1276	C−C stretch (interfluorene)
1231					in-plane CH bend
1196	1192				in-plane CH bend
1156					in-plane CH bend
1118	1138	1138	1138	1138	in-plane CH bend

Upon conjugation of fluorene units and IT core, the Raman spectral pattern changed as indicated in Figure 4. In the Raman spectra of ITF*n*, contributions of the vibrations due to fluorene units are observable at 1342−1345 and 1271−1276 cm^{-1}, which are attributable to intrafluorene C−C stretch (C−C stretch of the bond connecting two benzene rings in fluorene) and interfluorene C−C stretch (C−C stretch of the bond connecting two fluorene units), respectively. These bands were calculated to be 1334 and 1284 cm^{-1} for ITF2, respectively (Figure S4 in the Supporting Information).[23] Intensity of these oligofluorene-related bands becomes obvious with size of the star-shaped oligomer. The vibrations originated from fluorene units appearing at similar positions to those of TF*n* (Figure S3 in the Supporting Information).[19] On the other hand, the ITF*n* showed the most intense bands at 1601−1603 cm^{-1} and 1544−1546 cm^{-1} similar to IT. The theoretical calculation indicated that the 1601−1603 cm^{-1} band includes C−C stretch of fluorene unit (Figure S4 in the Supporting Information) as well as that of IT core, while vibration of the 1544−1546 cm^{-1} band is limited to the core. It should be noted that the 1544−1546 cm^{-1} band is intense while the corresponding peak of TF*n* is quite weak (Figure S3 in the Supporting Information) probably due to a symmetrical reason. This finding was reproduced by the theoretical calculation: The intensity of the 1544−1546 cm^{-1} band with respect to the 1601−1603 cm^{-1} band of ITF1 (ITF2) was calculated to be 0.63 (0.33) while that of TF1 (TF2) was 0.05 (0.02). The relative intensity of the 1544−1546 cm^{-1} band becomes smaller with the size of the oligomer because the 1601−1603 cm^{-1} band includes contributions of fluorene units in the branch of the star-shaped oligomer.

In order to study the Raman spectrum of radical ion species, various oxidation or reduction methods can be applied such as chemical and electrochemical methods. First, we applied chemical oxidizing agent ($SbCl_5$) to generate an oxidized oligomer,[24,25] but the attempt failed due to the difficulty in control of the oxidation states (cation and dication) because usually first and second oxidation potentials become close for

dx.doi.org/10.1021/jp412744p | J. Phys. Chem. A 2014, 118, 2307−2315

larger oligomers. In addition, possible dication formation from radical cations by disproportionation makes measurement difficult.[26] Thus, we employed TR^3 measurements during the pulse radiolysis of the sample. The present method is useful to follow the reaction processes of radical ions generated by pulse radiolysis. As indicated above, γ-ray radiolysis and pulse radiolysis of the present star-shaped oligomers generated radical cations which exhibit absorption in a wide spectral region range from the near-IR to UV regions. Since radical cations of TF*n*, ITF*n*, and CITF*n* showed substantial absorption at 532 nm, resonance condition can be achieved under the present experimental condition. On the other hand, absorbance of radical cations of T and IT at 532 nm is rather weak (Figure 3 and Figure S5 in the Supporting Information),[18] which resulted in poor signal-to-noise ratio of Raman spectra as shown Figure 4 and Figure S3 in the Supporting Information.

In the TR^3 spectrum of IT radical cation, the bands at 1590 and 1547 cm^{-1} appeared, which are the same vibrational modes as the 1600 and 1549 cm^{-1} bands of neutral IT, respectively. It is interesting to note that the shift due to the external benzene ring is larger than that of the inner benzene ring. This tendency was also confirmed by the theoretical calculation: The C−C stretching modes of the external and inner benzene rings in the oxidized form were calculated to be 1593 and 1541 cm^{-1} (neutral state: 1608 and 1546 cm^{-1}), respectively. The lower wavenumber shift of the largest peak around 1600 cm^{-1} was also confirmed with ITs conjugated with fluorene units. The peak was confirmed at 1591, 1592, 1594, and 1594 cm^{-1} for ITF1, ITF2, ITF3, and ITF4, respectively. The shift to the lower wavenumber of the present band can be attributed to the enhancement of quinoidal character upon oxidation, which has been reported for several oligomer system such as oligo-*p*-phenylene, TF*n*, and so on.[19,27−31] The contribution of quinoidal character is discussed in a later section.

Raman Spectra of CITF*n*. Raman spectra of neutral CITF*n* are shown in Figure 6. These Raman bands can be assigned as summarized in Table 4 on the basis of the assignments of Raman bands of ITF*n* and theoretical calculation (Figure 7). In the case of CITF1, the Raman bands attributable to C−C stretching of the external and inner benzene rings of IT core appeared at 1606 and 1543 cm^{-1}, respectively. It is indicated from the calculation that the 1606 cm^{-1} band includes three vibrational modes due to three branches of oligomer (calcd.: 1601, 1602, and 1603 cm^{-1}). In addition, the theoretical calculation predicted that the C−C stretching modes of the inner benzene rings of IT were 1565 and 1546 cm^{-1} (Figure 5), while corresponding modes of CITF1 were 1547 and 1540 cm^{-1}, respectively. In addition, the bands were calculated to be 1547 and 1537 cm^{-1} for CITF2 (Figure 7), respectively, indicating that difference in wavenumbers becomes smaller in CITF*n* when compared to that of IT. Thus, C−C stretching of the inner benzene of the core possibly appeared as a single peak (1543 cm^{-1} for CITF1), and the peak at 1566 cm^{-1} of CITF1 could be attributed to the one of the vibrations coupled to the external benzene rings of the core.

Vibrational modes due to the external benzene rings of the core tend to shift to the lower wavenumber side with the size of oligomer. This tendency was reproduced by the theoretical

Table 4. Observed Raman Bands of Neutral CITF*n* in DCE

CITF1	CITF2	CITF3	CITF4	assignment
1606	1602	1600	1599	C−C stretch
1566	1560	1555		C−C stretch
1543	1542	1541	1542	C−C stretch
1445				in-plane CH bend
1432	1425	1419	1417	in-plane CH bend
1362	1362	1363	1361	symmetric C−C stretch
1333				C−C stretch
1322	1328	1328	1323	C−C stretch
	1313	1310	1310	C−C stretch
1291	1291	1293		C−C stretch
1253	1253	1254	1252	in-plane CH bend
1207	1209			in-plane CH bend
1182	1180	1180	1179	in-plane CH bend
1152	1153	1154	1152	in-plane CH bend

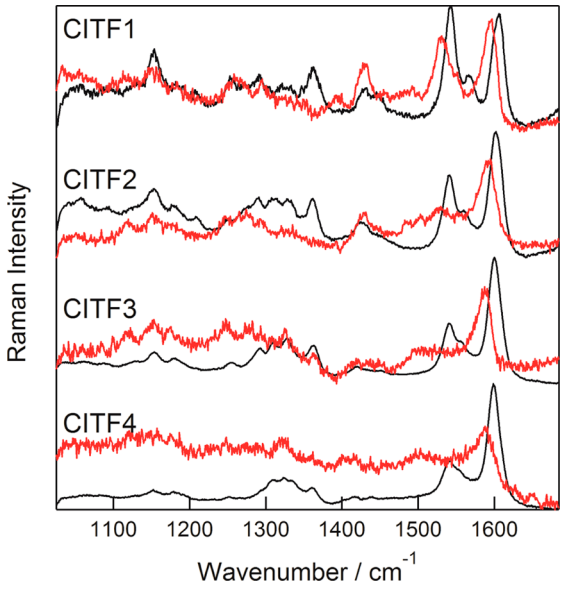

Figure 6. Raman spectra of neutral (black) and radical cation CITF*n* (red) in DCE. TR^3 spectra of radical cations were measured at 50 ns after electron pulse during the pulse radiolysis of CITF*n* in DCE.

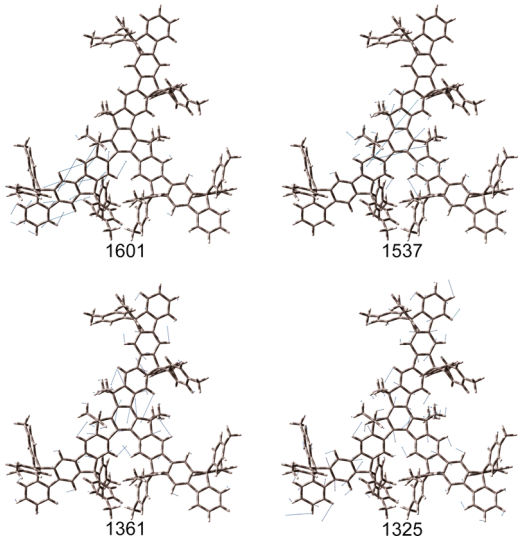

Figure 7. Representative atomic displacements of CITF2 calculated at the B3LYP/6-31G(d) level. Numbers under molecules are calculated wavenumbers scaled using a factor (0.97).

dx.doi.org/10.1021/jp412744p | J. Phys. Chem. A 2014, 118, 2307−2315

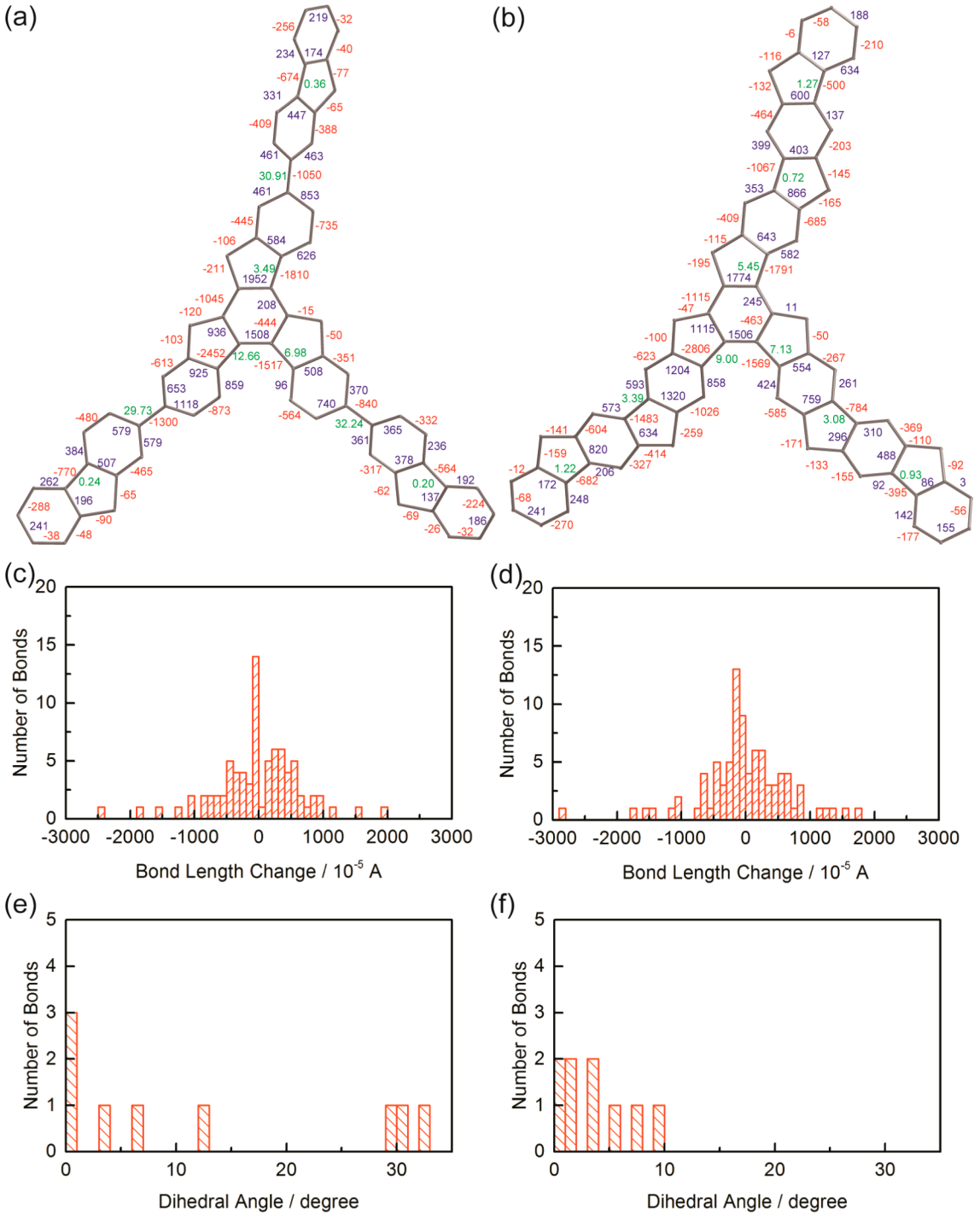

Figure 8. Structural change upon oxidation of ITF1 (anti form, a, c, and e) and CITF2 (b, d, and f) calculated at the B3LYP/6-31G(d) level. In (a) and (b), positive and negative bond length changes upon oxidation ((bond length in oxidized form) − (bond length in neutral form)) are indicated by blue and red numbers close to the bonds (unit: 10^{-5} Å), respectively. Numbers indicated by green are dihedral angle formed by benzene rings in the oxidized state. (c, d) Distribution of bond length change. (e, f) Distribution of dihedral angle in the oxidized form.

calculation. For example, one C−C stretching of external benzene rings of the core, which corresponds to the 1608 cm^{-1} mode in Figure 5, was calculated to be 1606 and 1601 cm^{-1} for CITF1 and CITF2, respectively (Figure 7). In addition, the symmetric C−C stretching mode of the central benzene ring of the IT core and C−C stretching connecting benzene rings of fluorene units of CITF*n* appeared at 1361−1363 and 1322−1328 cm^{-1}, respectively, which are lower wavenumbers compared to those of ITF*n* (1369−1372 and 1342−1345 cm^{-1}, respectively) and are reproduced by the theoretical calculation.

Raman spectra of the oxidized forms were also measured by means of the TR^3 spectroscopy during the pulse radiolysis as shown in Figure 6. In the case of larger CITF*n*, the formation of stable radical cation with recombination time longer than the pulse repetition prevented TR^3 measurement in better signal-to-noise ratio, because multiple irradiation caused sample damage. In the case of the radical cation of CITF*n*, the peak

dx.doi.org/10.1021/jp412744p | J. Phys. Chem. A 2014, 118, 2307−2315

position of the C−C stretching was 1597, 1595, 1587, and 1588 cm^{-1}, for CITF1, CITF2, CITF3, and CITF4, respectively, indicating the lower wavenumber shift due to enhancement of quinoidal character like the ITF*n* radical cation. The extent of the shift is 7−13 cm^{-1}, which is similar to that of ITF*n* (8−11 cm^{-1}) and TF*n* (8−13 cm^{-1}).

To gain better understanding on the observed Raman peak shift caused by the oxidation process, structural change upon oxidation was investigated on the basis of the theoretical calculation. Figure 8a,b shows structural change of ITF1 (all anti form) and CITF2, which include the same number of benzene rings in the oligomer backbone. Blue and red numbers close to the bonds indicate the positive and negative bond length changes upon oxidation, respectively. Structural change of ITF1 in the all syn form is indicated in Figure S6 in the Supporting Information. The largest bond length change was observed with the IT core in both cases. It should be noted that the bonds connecting the fluorene unit and the core become shorter upon oxidation. In addition, bonds connecting 1 and 9a, 3 and 4, and 4a and 4b positions of the fluorene unit also become shorter in the oxidized form, while other aromatic bonds become longer.[32] These structural changes indicate enhancement of quinoidal character. Histograms of bond length change are indicated in Figure 8c,d. Distribution of bond length changes of ITF1 and CITF2 are similar to each other. Similarity can be also confirmed by some statistic parameters: Standard deviation of the histogram of anti ITF1 (syn ITF1) and CITF2 was calculated to be 0.0068 (0.0068) and 0.0069 Å, respectively. In addition, the average of absolute value of bond length change was 0.0049 (0.0050) and 0.0048 Å, respectively. Thus, it can be concluded that the similar structural change of ITF1 and CITF2 caused the similar shift of the Raman peak around 1600 cm^{-1}.

In the previous paper, we indicated that the formation of radical cation of ITF*n* and TF*n* accompanied rotation of bonds connecting core and fluorene and those connecting fluorene and fluorene units to form a planar structure characteristic to enhanced quinoidal character.[18] The theoretical calculation predicted that the rotation of the bonds is about 5−6° in the cases of ITF1 and TF1, thus oligomers will not be a completely planar form upon oxidation. In Figure 8e, the distributions of the dihedral angles formed by the benzene rings connected by a single bond in the oxidized form are indicated. In the figure, bonds with ∼30° of dihedral angle can be attributed to those connecting core and fluorene unit, while others are bonds inside fluorene unit and core. On the other hand, in the case of CITF2 (Figure 8f), all dihedral angles are smaller than 10°, which is effective to the delocalization of the π-electron. Thus, the present study indicated that the planar structure of CITF*n* due to rigid oligomer backbone is quite important in extension of conjugation as revealed by the above absorption and fluorescence spectroscopic data.

CONCLUSIONS

In the present study, the radical cation of CITF*n*, star-shaped condensed oligofluorenes with IT core and fluorene unit, was investigated by means of radiation chemical methods. Absorption spectra of the radical cation of CITF*n* were measured in a wide spectral range. The observed absorption peaks are attributed to the electronic transitions adequately on the basis of TDDFT calculation. Among them, the strong visible absorption was attributed to the transition from HOMO to LUMO mainly, which exhibited a longer wavelength shift due to extended π-conjugation when compared to the corresponding ITF*n*. Furthermore, TR^3 spectra during the pulse radiolysis revealed the structural change upon oxidation due to enhancement of quinoidal character. Extent of enhanced quinoidal character, which was revealed by Raman peak shift around 1600 cm^{-1}, was similar to those of ITF*n* and TF*n*. This finding was reasonably explained by the theoretical calculation. Thus, it is indicated that a rigid oligomer framework which makes oligomer a planar structure is quite important in extension of the conjugation pathway.

ASSOCIATED CONTENT

Supporting Information

Molecular structures of TF*n* and ITF*n*, transient absorption spectra of CITF*n*, Raman spectra of TF*n*, atomic displacement of ITF2, absorption spectrum of T radical cation, structural change of syn ITF1, and complete author list of ref 21. This material is available free of charge via the Internet at http://pubs.acs.org.

AUTHOR INFORMATION

Corresponding Author

*E-mail: fuji@sanken.osaka-u.ac.jp; majima@sanken.osaka-u.ac.jp.

Notes

The authors declare no competing financial interest.

ACKNOWLEDGMENTS

We thank the members of the Research Laboratory for Quantum Beam Science of SANKEN, Osaka University, for running the linear accelerator. This work has been partly supported by a Grant-in-Aid for Scientific Research (Project 25220806, 25288035, and others) from the Ministry of Education, Culture, Sports, Science and Technology (MEXT) of Japanese Government. T.M. thanks the WCU (World Class University) program funded by the Ministry of Education, Science and Technology through the National Research Foundation of Korea (R31-2008-10035-0) for the support.

REFERENCES

(1) Leclerc, M. Polyfluorenes: Twenty Years of Progress. *J. Polym. Sci. A: Polym. Chem.* **2001**, *39*, 2867−2873.

(2) Pogantsch, A.; Wenzl, F. P.; List, E. J. W.; Leising, G.; Grimsdale, A. C.; Müllen, K. Polyfluorenes with Dendron Side Chains as the Active Materials for Polymer Light-Emitting Devices. *Adv. Mater.* **2002**, *14*, 1061−1064.

(3) Kulkarni, A. P.; Jenekhe, S. A. Blue Light-Emitting Diodes with Good Spectral Stability Based on Blends of Poly(9,9-Dioctylfluorene): Interplay between Morphology, Photophysics, and Device Performance. *Macromolecules* **2003**, *36*, 5285−5296.

(4) Gruber, J.; Li, R. W. C.; Aguiar, L. H. J. M. C.; Benvenho, A. R. V.; Lessmann, R.; Hummelgen, I. A. A Novel Soluble Poly-(Fluorenylenevinylene) Conjugated Polymer: Synthesis, Characterization and Application to Optoelectronic Devices. *J. Mater. Chem.* **2005**, *15*, 517−522.

(5) Belletête, M.; Ranger, M.; Beaupré, S.; Leclerc, M.; Durocher, G. Conformational, Optical and Photophysical Properties of a Substituted Terfluorene Isolated and Incorporated in a Polyester. *Chem. Phys. Lett.* **2000**, *316*, 101−107.

(6) Kanibolotsky, A. L.; Berridge, R.; Skabara, P. J.; Perepichka, I. F.; Bradley, D. D. C.; Koeberg, M. Synthesis and Properties of Monodisperse Oligofluorene-Functionalized Truxenes: Highly Fluorescent Star-Shaped Architectures. *J. Am. Chem. Soc.* **2004**, *126*, 13695−13702.

(7) Yang, J.-S.; Lee, Y.-R.; Yan, J.-L.; Lu, M.-C. Synthesis and Properties of a Fluorene-Capped Isotruxene: A New Unsymmetrical Star-Shaped π-System. *Org. Lett.* **2006**, *8*, 5813−5816.
(8) Yang, J.-S.; Huang, H.-H.; Ho, J.-H. Electronic Properties of Star-Shaped Oligofluorenes Containing an Isotruxene Core: Interplay of Para and Ortho Conjugation Effects in Phenylene-Based π Systems. *J. Phys. Chem. B* **2008**, *112*, 8871−8878.
(9) Yang, J.-S.; Huang, H.-H.; Lin, S.-H. Facile Multistep Synthesis of Isotruxene and Isotruxenone. *J. Org. Chem.* **2009**, *74*, 3974−3977.
(10) Yang, J.-S.; Huang, H.-H.; Liu, Y.-H.; Peng, S.-M. Synthesis and Electronic Properties of Isotruxene-Derived Star-Shaped Ladder-Type Oligophenylenes: Bandgap Tuning with Two-Dimensional Conjugation. *Org. Lett.* **2009**, *11*, 4942−4945.
(11) Huang, H.-H.; Prabhakar, C.; Tang, K.-C.; Chou, P.-T.; Huang, G.-J.; Yang, J.-S. Ortho-Branched Ladder-Type Oligophenylenes with Two-Dimensionally π-Conjugated Electronic Properties. *J. Am. Chem. Soc.* **2011**, *133*, 8028−8039.
(12) Omer, K. M.; Kanibolotsky, A. L.; Skabara, P. J.; Perepichka, I. F.; Bard, A. J. Electrochemistry, Spectroscopy, and Electrogenerated Chemiluminescence of Some Star-Shaped Truxene−Oligofluorene Compounds. *J. Phys. Chem. B* **2007**, *111*, 6612−6619.
(13) Hernandez-Santana, A.; Mackintosh, A. R.; Guilhabert, B.; Kanibolotsky, A. L.; Dawson, M. D.; Skabara, P. J.; Graham, D. Dip-Pen Nanolithography of Nanostructured Oligofluorene Truxenes in a Photo-Curable Host Matrix. *J. Mater. Chem.* **2011**, *21*, 14209−14212.
(14) Fujitsuka, M.; Cho, D. W.; Huang, H.-H.; Yang, J.-S.; Majima, T. Structural Relaxation in the Singlet Excited State of Star-Shaped Oligofluorenes Having a Truxene or Isotruxene as a Core. *J. Phys. Chem. B* **2011**, *115*, 13502−13507.
(15) Montgomery, N. A.; Denis, J.-C.; Schumacher, S.; Ruseckas, A.; Skabara, P. J.; Kanibolotsky, A.; Paterson, M. J.; Galbraith, I.; Turnbull, G. A.; Samuel, I. D. W. Optical Excitations in Star-Shaped Fluorene Molecules. *J. Phys. Chem. A* **2011**, *115*, 2913−2919.
(16) Montgomery, N. A.; Hedley, G. J.; Ruseckas, A.; Denis, J.-C.; Schumacher, S.; Kanibolotsky, A. L.; Skabara, P. J.; Galbraith, I.; Turnbull, G. A.; Samuel, I. D. W. Dynamics of Fluorescence Depolarisation in Star-Shaped Oligofluorene-Truxene Molecules. *Phys. Chem. Chem. Phys.* **2012**, *14*, 9176−9184.
(17) Belton, C. R.; Kanibolotsky, A. L.; Kirkpatrick, J.; Orofino, C.; Elmasly, S. E. T.; Stavrinou, P. N.; Skabara, P. J.; Bradley, D. D. C. Location, Location, Location - Strategic Positioning of 2,1,3-Benzothiadiazole Units within Trigonal Quaterfluorene-Truxene Star-Shaped Structures. *Adv. Funct. Mater.* **2013**, *23*, 2792−2804.
(18) Fujitsuka, M.; Tojo, S.; Yang, J.-S.; Majima, T. γ-Ray Radiolysis and Theoretical Study on Radical Ions of Star-Shaped Oligofluorenes Having a Truxene or Isotruxene as a Core. *Chem. Phys.* **2013**, *419*, 118−123.
(19) Moreno Oliva, M.; Casado, J.; López Navarrete, J. T.; Berridge, R.; Skabara, P. J.; Kanibolotsky, A. L.; Perepichka, I. F. Electronic and Molecular Structures of Trigonal Truxene-Core Systems Conjugated to Peripheral Fluorene Branches. Spectroscopic and Theoretical Study. *J. Phys. Chem. B* **2007**, *111*, 4026−4035.
(20) Shida, T. *Electronic Absorption Spectra of Radical Ions*; Elsevier: New York, 1988.
(21) Frisch, M. J.; Trucks, G. W.; Schlegel, H. B.; Scuseria, G. E.; Robb, M. A.; Cheeseman, J. R.; Scalmani, G.; Barone, V.; Mennucci, B.; Petersson, G. A. et al. *Gaussian 09, Revision A.02*; Gaussian, Inc.: Wallingford, CT, 2009.
(22) Ie, Y.; Endou, M.; Lee, S. K.; Yamada, R.; Tada, H.; Aso, Y. Completely Encapsulated Oligothiophenes: Synthesis, Properties, and Single-Molecule Conductance. *Angew. Chem., Int. Ed.* **2011**, *50*, 11980−11984.
(23) Tsoi, W. C.; Lidzey, D. G. Raman Spectroscopy of Fluorene Oligomers in the α-, β- and γ-Phases. *J. Phys.: Condens. Matter* **2008**, *20*, 125213.
(24) Heckmann, A.; Amthor, S.; Lambert, C. Mulliken-Hush Analysis of a Bis(Triarylamine) Mixed-Valence System with a NN Distance of 28.7 Å. *Chem. Commun.* **2006**, 2959−2961.
(25) Cho, N.; Zhou, G.; Kamada, K.; Kim, R. H.; Ohta, K.; Jin, S.-H.; Mullen, K.; Lee, K.-S. The Impact of Charge Defects and Resonance Enhancement on the Two-Photon Absorption Activity of Spirofluorene and Ladder-Type Pentaphenylene Derivatives. *J. Mater. Chem.* **2012**, *22*, 185−191.
(26) Zade, S. S.; Zamoshchik, N.; Bendikov, M. From Short Conjugated Oligomers to Conjugated Polymers. Lessons from Studies on Long Conjugated Oligomers. *Acc. Chem. Res.* **2010**, *44*, 14−24.
(27) Furukawa, Y.; Ohtsuka, H.; Tasumi, M.; Wataru, I.; Kanbara, T.; Yamamoto, T. Raman Studies of Intact and Sodium Doped ^{13}C-Substituted Poly-p-Phenylene. *J. Raman Spectrosc.* **1993**, *24*, 551−554.
(28) Sakamoto, A.; Furukawa, Y.; Tasumi, M. Resonance Raman Characterization of Polarons and Bipolarons in Sodium-Doped Poly(p-Phenylenevinylene). *J. Phys. Chem.* **1992**, *96*, 3870−3874.
(29) Ponce Ortiz, R.; Casado, J.; Rodríguez González, S.; Hernández, V.; López Navarrete, J. T.; Viruela, P. M.; Ortí, E.; Takimiya, K.; Otsubo, T. Quinoidal Oligothiophenes: Towards Biradical Ground-State Species. *Chem.—Eur. J.* **2010**, *16*, 470−484.
(30) Casado, J.; Ponce Ortiz, R.; Lopez Navarrete, J. T. Quinoidal Oligothiophenes: New Properties Behind an Unconventional Electronic Structure. *Chem. Soc. Rev.* **2012**, *41*, 5672−5686.
(31) Fujitsuka, M.; Iwamoto, T.; Kayahara, E.; Yamago, S.; Majima, T. Enhancement of the Quinoidal Character for Smaller [n]-Cycloparaphenylenes Probed by Raman Spectroscopy. *ChemPhysChem* **2013**, *14*, 1570−1572.
(32) Fratiloiu, S.; Grozema, F. C.; Koizumi, Y.; Seki, S.; Saeki, A.; Tagawa, S.; Dudek, S. P.; Siebbeles, L. D. A. Electronic Structure and Optical Properties of Charged Oligofluorenes Studied by Vis/Nir Spectroscopy and Time-Dependent Density Functional Theory. *J. Phys. Chem. B* **2006**, *110*, 5984−5993.